Estuarine, Coastal and Shelf Science 205 (2018) 40–45

Contents lists available at ScienceDirect

Estuarine, Coastal and Shelf Science

journal homepage: www.elsevier.com/locate/ecss

High resolution LiDAR measurements reveal fine internal structure and variability of sediment-carrying coastal plume

P.O. Zavialov [a, *], V.V. Pelevin [a], N.A. Belyaev [a], A.S. Izhitskiy [a], B.V. Konovalov [a], V.V. Krementskiy [a], I.V. Goncharenko [a], A.A. Osadchiev [a], D.M. Soloviev [a, b], C.A.E. Garcia [c], E.S. Pereira [d], L. Sartorato [c], O.O. Moller Jr. [d]

[a] P.P. Shirshov Institute of Oceanology, Russian Academy of Sciences, Russia
[b] Marine Hydrophysical Institute, Russian Academy of Sciences, Russia
[c] Federal University of Santa Catarina, Brazil
[d] Federal University of Rio Grande, Brazil

ARTICLE INFO

Article history:
Received 21 September 2017
Received in revised form
30 December 2017
Accepted 8 January 2018
Available online 11 January 2018

ABSTRACT

We report results of a field survey conducted in the buoyant, sediment-carrying coastal plume generated by the discharge from the Patos Lagoon, the World's largest choked lagoon. The concentration of total suspended matter (TSM) and organic matter (as represented by total organic carbon, TOC) were mapped using an ultraviolet fluorescent LiDAR, which allowed for extensive data coverage (total of 79,387 simultaneous determinations of TSM and TOC) during 3 consecutive days. These observations were accompanied by hydrographic measurements from the ship and at a mooring station. We first describe synoptic variability of the plume, which responded energetically to wind forcing. We then analyze the TSM, TOC and hydrographic data jointly and develop a simple approach to estimate the rates of suspended matter removal from the upper layer due to gravitational settling and turbulent mixing based on relative changes in TSM and TOC concentrations. Four distinct regions within the plume exhibiting different dynamics of suspended and dissolved constituents were identified on this basis.

1. Introduction

As major mediators of continent-sea exchanges, river plumes in coastal ocean have been subject to extensive studies [see, for example, a recent review paper by Horner-Devine et al. (2015)], However, as pointed out in the review, "*although these studies have clarified many individual processes, a holistic description of the interaction and relative importance of different mixing and transport processes in river plumes has not yet been realized*". This is so partly because observational data at spatial and temporal resolution sufficient to elucidate the internal structure and variability of plumes, especially those of modest sized rivers, are rare. In the case study reported in this research note, we took advantage of using high resolution optical instrument to address this issue in the area adjacent to the Patos Lagoon mouth on the South Brazilian shelf. We report results of a field campaign where, thanks to a novel ultraviolet fluorescent LiDAR, we were able to measure the concentrations of total suspended matter (TSM) and total organic carbon (TOC) in the Patos lagoon plume area at high spatial resolution and extensive data coverage virtually inaccessible to other observational methods. Therefore, the primary objective of ths paper is to describe the fine internal structure of a coastal plume with the emphasis given to TSM and TOC concentration fields in their relations with the thermohaline structure.

The Patos Lagoon is the second most important source of continental freshwater discharges and terrigeneous sediment loads on the shelf of Southwestern Atlantic, after the Plata Estuary located some 400 km south, so that the Patos plume is essentially embedded in the larger Plata plume (Zavialov et al., 2003, Burrage et al., 2008). In most cases, the Patos plume extends to about 20 km offshore and occupies an area of approximately 1500 km^2 (Fernandes et al., 2002), but other figures ranging from 10 km to 55 km have also been reported (e.g., Zavialov et al., 2003). Recent numerical studies examined the roles of different forcing factors in the general dynamics of the plume (Marques et al., 2009, Marques et al., 2010, Kirinus et al., 2012). However, relatively little is known

* Corresponding author.
E-mail address: peter@ocean.ru (P.O. Zavialov).

https://doi.org/10.1016/j.ecss.2018.01.008
0272-7714/

about the internal structure and synoptic variability of the Patos plume, especially from the observational standpoint.

The runoff from the lagoon carries large volumes of fine sediments, as well as dissolved and particulate organic matter (Calliari et al., 2008, Kirinus et al., 2012). The total export of suspended material is estimated as about $1.4 \cdot 10^7$ tonnes per year (Marques et al., 2010). These discharges sometimes trigger negative consequences, such as massive depositions of mud on nearby beaches in the popular Cassino Beach resort area, south of the lagoon mouth, deteriorating their recreational potential (Calliari et al., 2008, Silva et al., 2015). Anthropogenic factors such as dredging of the lagoon entrance and dumping of the removed sediment at incorrectly selected sites also add to these processes (Calliari et al., 2001).

2. Material and methods

The data used in this study were collected on the shelf adjacent to the outlet of the Patos Lagoon, the World's largest chocked lagoon, situated at the Atlantic coast of South America at 30-32°S. Fed by the Guaíba River, the Camaquã River, and several smaller rivers, it drains the runoff from its catchment of over 200,000 km^2 into the ocean. The lagoon outlet is protected by two partially permeable stone jetties, about 4 km long each, built in 1907 and renovated in 2015 (Silva et al., 2015). The long-term average discharge from the lagoon is 2088 m^3 s^{-1} (Marques et al., 2010), albeit peak values up to 25,000 m^3 s^{-1} have been documented, especially under rainy conditions associated with El-Nino events (e.g., Fernandes et al., 2002).

The field campaign was conducted onboard R/V Larus of the Federal University of Rio Grande on November 29 through December 2, 2016.

Daily measurements were conducted from the ship, comprising continuous soundings along the ship's track using an ultraviolet fluorescent LiDAR *UFL-9* that measured bulk concentrations of TSM (including particles of all sizes above 0.45 μm) and TOC. The LiDAR emits laser ray at 355 nm wavelength, which excites fluorescence of constituents dissolved or suspended in water. The fluorescence spectrum is then analyzed to obtain concentrations of organic carbon (around 440 nm) and chlorophyll (685 nm), as well as suspended matter derived from Raman scattering at 405 nm. Details of the instrument and its application are described in (Palmer et al., 2013, Pelevin et al., 2017). Some examples of using LiDAR for detecting river plumes are given in (Osadchiev et al., 2017).

The depth up to which the laser ray penetrates into water depends on turbudity, but, generally, is considered to be about 1 m, hence, all data collected by the *UFL-9* correspond to this uppermost 1 m portion of the water column. The sampling rate of 2 Hz allowed for extensive data coverage (in the present study, 79,387 data distributed over the study region during 4 days).

Calibration against the *in situ* data is required for every use of the UFL-9 (Pelevin et al., 2017). In this case, 26 water samples analyzed (14 for total suspended matter and 12 for total organic carbon) were utilized for this purpose. The samples were analyzed in laboratory using standard techniques (filter weighting for TSM, *Shimadzu* analyzer for TOC). The LiDAR-derived and the *in situ* data demonstrated reasonably good agreement, with the relative root-mean-square error amounting to 26% for TSM and only 12% for TOC. The determination coefficients R^2 for the respective regressions were 0.85 and 0.79. The maximum errors registered in this set of samples were 38% for TSM and 32% for TOC.

The LiDAR measurements were accompanied by standard hydrographic measurements from the ship (accompanied with CTD profiling by *JFE Advantech Rinko* instrument, and water sampling at 4–8 stations per day) and at a mooring station located close to the estuary entrance. The mooring station was deployed at the depth of 12.5 m at 17:40 (local time) on November 29 and recovered at 15:50 on December 2, so the total duration of measurements at the station was 70 h 10 min. The location of the mooring station is shown by the green triangle in Fig. 1.

The mooring station was equipped with *StarOddi* thermistors fixed at 4.5 m, 6.5 m, 7.5 m, 8.5 m, 10.5 m, and 12.5 m depth levels. The lowermost thermistor had also a pressure sensor. A *TSM*-type tilt current meter was installed on the bottom at the depth of 12.5 m. The sampling rate was set to 2 min for the thermistors and to 10 min for the current meter. In addition, hourly wind data were obtained from the meteostation operated by the Rio Grande port authorities at the site called Praticagem shown by the green bullet in Fig. 1.

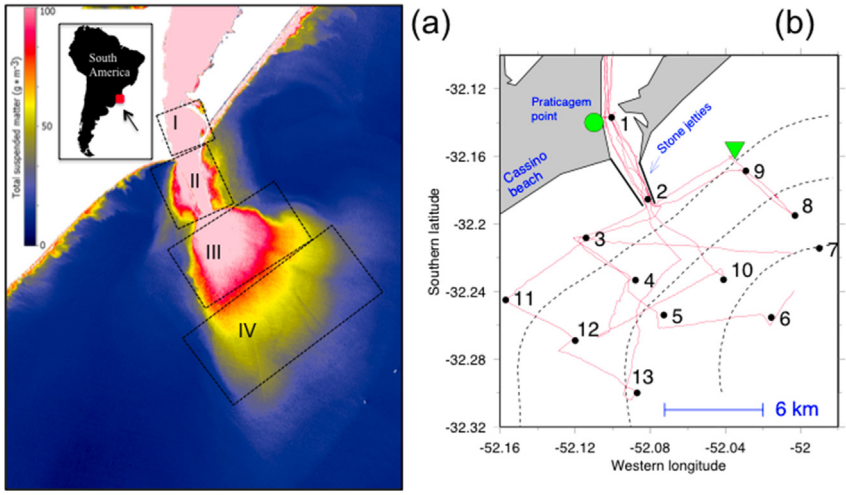

Fig. 1. (a) TSM concentration field as obtained from satellite image of Sentinel-2A (MSI) radiometer taken on December 6, 2016, showing the Patos plume after the end of the field campaign. The boxes superimposed on the image and identified by Roman numbers are distinct regions of the plume as explained in the text; (b) Daily LiDAR measurements along the ship's track (red curve), CTD and water sampling stations (black bullets), and the locations of the mooring station (green triangle) and meteorological station (green bullet). The dashed contours indicate the 5 m, 10 m, and 15 m isobaths based on ETOPO1 bathymetry. (For interpretation of the references to colour in this figure legend, the reader is referred to the Web version of this article.)

3. Results and discussion

3.1. Temporal variability of the plume

Panels (a)-(c) of Fig. 2 show the changes in wind forcing during the study period along with the response of the ocean current at the bottom underneath the plume, as well as the thermal stratification and the bottom pressure.

The analysis of the data series revealed that the alongshore current velocity was highly correlated (r up to 0.9) with the

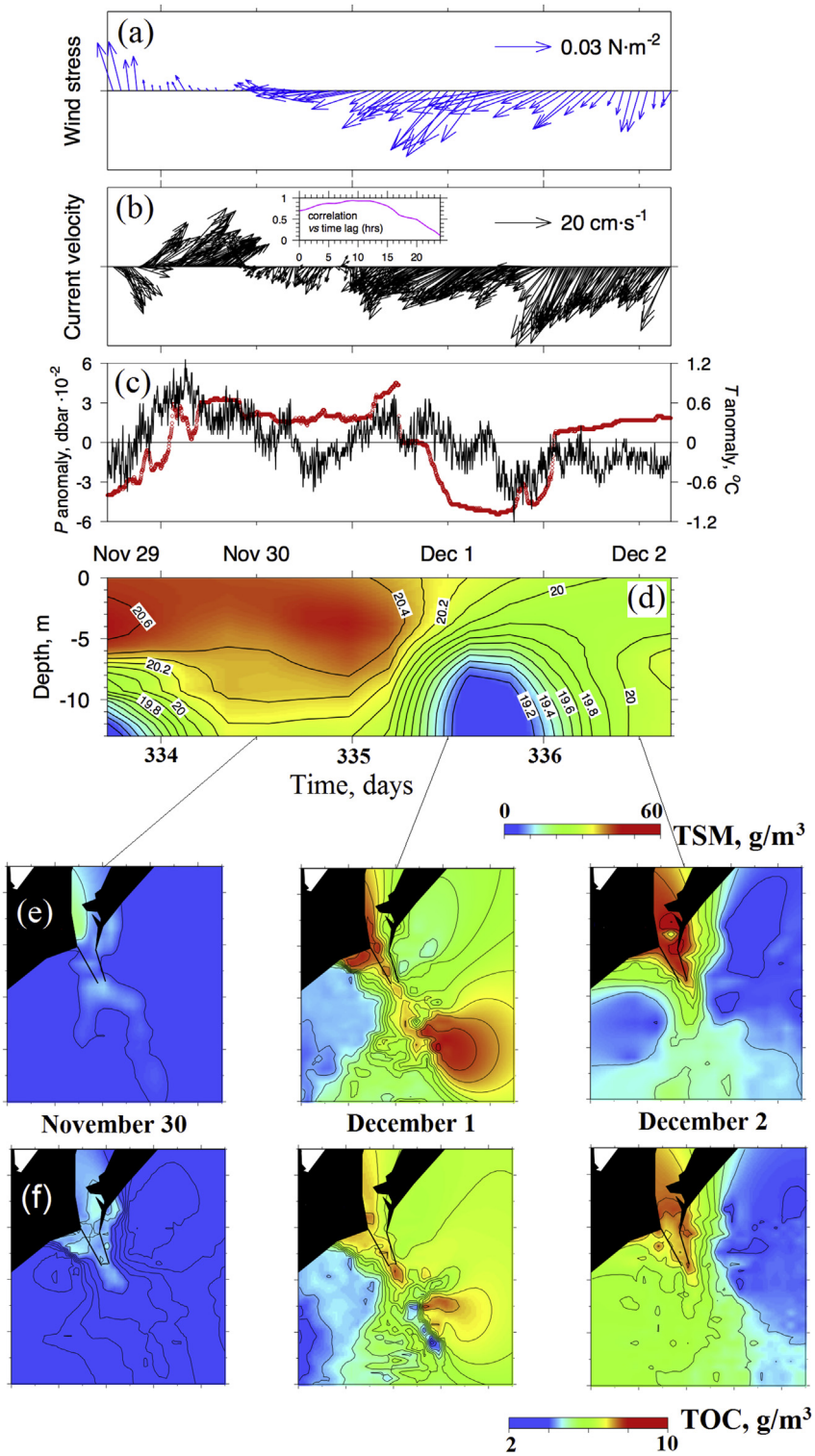

Fig. 2. Temporal variability during the period of the moored measurements. (a) - wind stress ($N \cdot m^{-2}$); (b) - current velocity ($cm \cdot s^{-1}$) in the bottom layer (the small inner frame exhibits the correlation coefficient between the alongshore wind stress and the alongshore current as function of the time lag, hours); (c) - bottom temperature anomaly (^{o}C, red) and bottom pressure anomaly (10^{-2} dbar, black); (d) - depth-time plot of temperature variability as recorded by the thermistor chain; (e) - TSM and (f) - TOC concentrations obtained from the UFL measurements on November 30 (left), December 1 (center), and December 2, 2016 (right). (For interpretation of the references to colour in this figure legend, the reader is referred to the Web version of this article.)

alongshore wind stress. The maximum correlation corresponded to the time lag of about 8 h (see Fig. 2b, inner frame). Other velocity components exhibited no correlations.

The bottom pressure anomaly (Fig. 2c), i.e., the demeaned value, was correlated with the wind stress at the scales of hours to days, reflecting wind-controlled changes of the sea level. Another interesting feature evident in the pressure record is the presence of high frequency oscillation that is visibly manifested in the time series. Spectral analysis (not shown) indicated that this oscillation corresponded to the periods of 10–20 min. Hypothetically, it could be attributed to short-period internal waves triggered by non-stationary river plume and developing on plume-generated stratification as observed in other estuarine areas (e.g., Nash and Moum, 2005).

On November 29 and the first half of November 30, the south and southeast winds prevailed driving waters northward and essentially pumped ocean water into the lagoon inlet at up to 30 cm s^{-1}. However, even under these conditions of rather intense onshore flow, there still did exist a hint of the lagoon plume manifested as a limited area of slightly but distinctly elevated TSM and TOC concentrations extending to a considerable distance oceanward (Fig. 2e and f).

On December 1, the wind became stronger and changed its direction to northeasterly. This resulted in reversal of the current direction to the southwest and created an upwelling-type circulation. Indeed, an abrupt water temperature drop by over 1 °C propagating upwards from the bottom (Fig. 2d) is clearly indicative of a developing upwelling event. The Patos plume as manifested in both TSM and TOC attained its maximum spatial extent with the general tendency to veer offshore and left with respect to the mouth, perhaps due to the Ekman action of relatively strong winds, although its internal structure was irregular and patchy. It is well known that buoyant plumes respond energetically on changes in wind forcing, e.g., (Li et al., 2017). On December 2, the plume propagated offshore and southwestward from the mouth. The wind changed its direction from NE to N and weakened, and the upwelling ceased as quickly as it had appeared. The transient upwelling event left the water column almost uniform, which is in agreement with previous studies pointing on enhancement of mixing within and beneath river plumes during upwellings (Fong and Geyer, 2001).

3.2. Composite internal structure of the plume

Our objective is to retain features that are common for different forcing situations as discussed above, so the observational data presented in this subsection were averaged over the 3 consecutive days from November 30 through December 2, 2016. Furthermore, TSM and TOC concentration values attributed to distance L as shown in Fig. 3 were obtained by averaging all (previously gridded) *UFL-9* data whose distance to the lagoon entrance belonged to the interval $[L, L+\Delta L]$, where ΔL was set to 200 m. The lagoon entrance, i.e., the point where $L = 0$, was set to correspond to the center of the channel at the Praticagem point.

Both TSM and TOC concentrations exhibited their maxima of 32 g m^{-3} and 6 g m^{-3}, respectively, at $L = 0$. At the periphery of the plume, the TSM and TOC concentrations spanned around 10 g m^{-3} and 4 g m^{-3}.

The brown triangles in Fig. 3 represent the TSM/TOC ratio, which holds information about relative roles of turbulent mixing versus gravitational settling in removal of terrigeneous suspended matter from the uppermost layer of the water column.

Consider the theoretical situation where the Patos Lagoon discharge is the major source of TSM and TOC in the study area, and

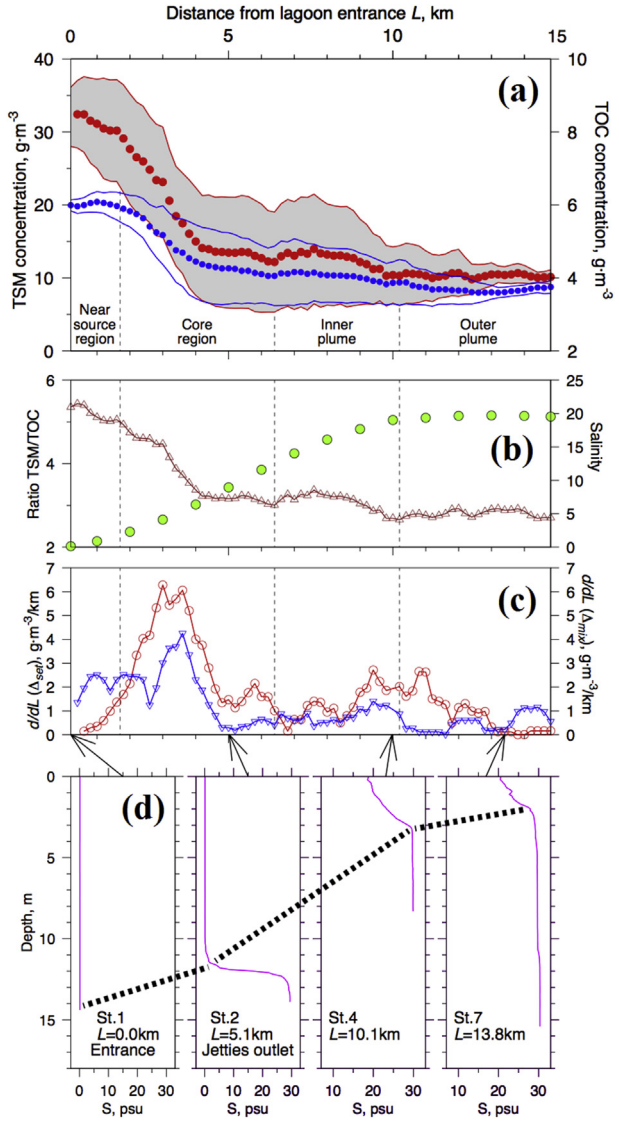

Fig. 3. Composite internal structure of the plume as function of distance from the lagoon entrance (Praticagem point). (a) - Concentrations of TSM (red bullets) and TOC (blue bullets). Intervals indicated by thin lines are rms deviations; (b) - Salinity (green bullets) and ratio TSM/TOC (brown triangles); (c) – Functions $\frac{d}{dL}\Delta_{\mathrm{mix}}$ (red circles) and $\frac{d}{dL}\Delta_{\mathrm{set}}$ (blue triangles) as explained in the text; (d) - Examples of surface-to-bottom salinity profiles recorded at Stations 1, 2, 4, and 7 on December 2, 2016. The dashed lines schematize the spatial structure of the plume thickness. (For interpretation of the references to colour in this figure legend, the reader is referred to the Web version of this article.)

other sources are negligible. Further, we assume that any unit volume Lagrangian water parcel observed at the distance L from the lagoon entrance and characterized by the concentrations TSM_L and TOC_L represents a product of turbulent mixing between the volume (*1-q*) of the continental water discharged from the lagoon with the initial concentrations TSM_0 and TOC_0 on the one hand, and the volume q of the ambient ocean water where both concentrations of TSM and TOC are small and negligible with respect to TSM_0 and TOC_0 on the other.

In this case, the ratio TSM/TOC would be constant, and

$$TSM_L = (1 - q)TSM_0, \quad (1)$$

where

$$q = \frac{TOC_0 - TOC_L}{TOC_0}.$$

However, in almost all real observations, the factually measured concentrations TSM_L and TOC_L are such that TSM_L is smaller than that prescribed by equation (1). This can be explained by the fact that while the concentration of terrigeneous dissolved organic matter decreases mainly because of dilution, i.e., mixing, the suspended solid matter is also subject to dilution, but, in addition, is removed from the surface layer by gravitational settling. Therefore, the cumulative "loss" of TSM from the water parcel due to settling can be estimated as $\Delta_{set} = (1-q)TSM_0 - TSM_L$ while that due to turbulent mixing with the ambient ocean water is $\Delta_{mix} = qTSM_0$. Differentiating these dependencies with respect to the distance L, we then obtain the proxies for the spatial densities of settling and mixing, which can be interpreted as the concentration decrease per unit length of the water parcel's path.

Of course, this model is overly simplified, as it ignores the possibility of other sources of organic carbon and suspended matter supply to the upper layer, such as resuspension from the bottom, for example. This can be partly justified by turbidity profiles (not shown) registered during the field campaign indicating that the role of resuspension was restricted to the near-bottom layer. Furthermore, TSM and TOC are treated here as passive tracers controlled by hydrodynamic factors, while all potential biogeochemical contributors to TSM and TOC budgets are neglected. Despite these obvious drawbacks, the approach may represent reasonably well the intrinsic general relations between suspended and dissolved tracers of river discharges, and, therefore, be insightful. Therefore, the functions $\frac{d}{dL}\Delta_{mix}$ and $\frac{d}{dL}\Delta_{set}$ shown in Fig. 3 are interpreted here as estimates for the spatial rates of TSM removal from the uppermost layer of the column due to turbulent mixing and gravitational settling, respectively.

As it is seen in Fig. 3, TSM loss due to mixing generally prevails over settling, exceeding the latter by a factor of 1.52 on the overall average. This is the case almost everywhere, except the immediate proximity (about 2 km) of the lagoon entrance where the situation is opposite. Farther offshore mixing grows and eventually becomes more important than settling, however, both mixing and settling increase with the distance from the lagoon entrance and simultaneously attain their maximum values at 3–5 km from the coast. Oceanward of this area, both mixing and settling intensities drop rather abruptly. However, as the distance increases further, settling remains small (although nonzero, even 15 km away from the shore), while mixing demonstrates another moderate increase at the distance of 9–11 km, and only then tends to small values. Note that this secondary intensification of mixing coincides with the area where the salinity dependence on distance from the shore demonstrates inflection suggesting a boundary between the inner and the outer portions of the plume and, possibly, velocity shear.

The example CTD profiles in Fig. 3 (bottom panel) indicate a transition from fresh and fully mixed water column near the lagoon entrance (which explains why no TSM removal by mixing occurred in this region) to a stepwise stratification near the outlet between the jetties, followed by shallowing of the freshwater-affected layer oceanward, fast at first and then slow, to salinities above 20 in the outer parts of the plume.

The numbers given in Table 1 were computed through direct integration of the data presented in Fig. 3. Based on these data, we can identify 4 distinct structural parts of the Patos Lagoon plume exhibiting different dynamics of TSM and TOC as well as thermohaline properties (Table 1). The respective regions are also distinct in satellite imagery (see Fig. 1a).

4. Conclusions

The fluorescent LiDAR measurements calibrated for TSM and TOC concentrations accompanied by hydrographic and optical measurements in the Patos Lagoon's coastal plume yielded new information about the synoptic variability and internal structure of the plume at high along-track spatial resolution and extensive data coverage virtually inaccessible for other observational methods.

The plume responded energetically on wind forcing changes at subdiurnal temporal scales with the maximum correlation corresponding to the time lag of 8 h. Transient wind-driven coastal upwelling event contributed significantly to the ocean temperature variability in the plume area during the study period. The sea bottom pressure recorded underneath the plume pointed on the presence of the short-period (10–20 min) internal waves.

Joint analysis of TSM and TOC data based on TSM/TOC ratio allowed obtaining insights into the internal structure of the plume. The bulk TSM removal from the surface layer due to turbulent mixing generally exceeded that due to settling by a factor of 1.6, on average, except at about 2 km wide area immediately adjacent to the entrance, where the situation was the opposite.

Four distinct regions of the plume were identified with respect to variability of TOC and TSM concentrations: the fully mixed "near-source" region (0–2 km from the lagoon entrance) where concentrations were maximum and TSM settling prevailed; the stratified "core" region of the plume (2–6 km) where TSM and TOC concentrations were subject to abrupt decrease mainly due to turbulent mixing with surrounding waters; the "inner" plume characterized by elevated spatial variability and patchiness of both TSM and TOC fields, significant increase of salinity and shallowing of the plume oceanward; and more uniform "outer" plume. The near-source region whose area was less than 2% of the total plume

Table 1
Identified regions of the plume and their characteristics with respect to the TSM and the TOC variability.

	Region	Distance from the source, range (km)	Description	Area (% of the total plume area)	TSM content (% of the overall TSM content in the plume)	TOC content (% of the overall TOC content in the plume)	Suspended material settling (% of the overall TSM loss in the plume)	Suspended material removal due to mixing (% of the overall TSM loss in the plume)
I	Near-source	0–2	No stratification. Salinity close to zero.	2	27	19	10	4
II	Core	2–6	Stratification develops in the bottom layer.	15	30	28	17	34
III	Inner plume	6–11	Shallowing of the plume-affected layer and increase of salinity oceanward.	38	24	31	8	17
IV	Outer plume	>11	Salinity and thickness of the plume-affected layer almost uniform.	45	19	22	5	5

area contained 27% of TSM and 19% of TOC and accounted for about 14% of TSM removal from the surface layer, mainly because of gravitational settling. The “core” part of the plume within the jetties and outside them at distances less than 1 km from the outlet was responsible for about 30% of both TSM and TOC contents and over 50% of TSM loss, mainly due to turbulent mixing. Another 25% of TSM withdrawal from the upper layer occurred in the “inner” part of the plume at the distances 6–11 km from the lagoon entrance, and only 10% of the loss took place beyond this distance - even though this “outer” part of the plume occupied almost half of the plume area.

In our opinion, combining high resolution measurements with joint analysis of suspended and dissolved tracers as exemplified in this research note represents a potentially promising new approach to investigating river plumes and associated sediment flows. Future research by means of both observations and modeling will help to obtain more comprehensive insights into the fine internal structure and synoptic variability of the Patos Lagoon plume and other sediment-carrying coastal plumes in the ocean.

Acknowledgments

The authors thank the master and the crew of R/V Larus. The field work was supported by the Russian Science Foundation (Grant 14-50-00095), while the data analyses and preparation of the publication were performed in the framework of the state assignment of FASO Russia (theme No. 0149-2018-0002). C.G. wishes to acknowledge support from Brazilian National Council for Scientific and Technological Development (CNPq), project No. 428039/2016-2. O.M.Jr wishes to acknowledge support from CNPq (project 305295/2013-6) and Inter-American Institute for Global Change Research (IAI), grant CRN 3070.

References

Burrage, D., Wesson, J., Martinez, C., Perez, T., Moller Jr., O., Piola, A., 2008. Patos Lagoon outflow within the Rio de la Plata plume using an airborne salinity mapper: observing an embedded plume. Continent. Shelf Res. 28, 1625–1638. https://doi.org/10.1016/j.csr.2007.02.14.

Calliari, L.J., Winterwerp, J.C., Fernandes, E., Cuchiara, D., Vinzon, S.B., Sperle, M., Holland, K.T., 2008. Fine grain sediment transport and deposition in the Patos Lagoon-Cassino beach sedimentary system. Continent. Shelf Res. https://doi.org/10.1016/j.csr.2008.09.019.

Calliari, L.J., Speranski, N.S., Torroteguy, M., Oliveira, M.B., 2001. The mud banks of Cassino beach, southern Brazil: characteristics, processes and effects. J. Coast Res. 34, 318–325.

Fernandes, E.H.L., Dyer, K.R., Moller, O.O., Niencheski, L.F.H., 2002. The Patos lagoon hydrodynamics during an El Nino event (1998). Continent. Shelf Res. 22, 1699–1713.

Fong, D.A., Geyer, W.R., 2001. Response of a river plume during an upwelling favorable wind event. J. Geophys. Res. 106 (C1), 1067–1084. https://doi.org/10.1029/2000JC900134.

Horner-Devine, A.R., Hetland, R.D., MacDonald, D.G., 2015. Mixing and transport in coastal river plumes. Annu. Rev. Fluid Mech. 47, 569–594. https://doi.org/10.1146/annurev-fluid-010313-141408.

Kirinus, E.P., Marques, W.C., Costa, J.C., Fernandes, E.H.L., 2012. The contribution of waves in mixing processes of the Patos Lagoon plume. Int. J. Geosci. 3, 1019–1026. https://doi.org/10.4236/ijg.2012.35102.

Li, Y., Martins, F., Wolanski, E., 2017. Sensitivity analysis of the physical dynamics of the fly river plume in Torres strait. Estuar. Coast Shelf Sci. 194, 84–91. https://doi.org/10.1016/j.ecss.2017.06.006.

Marques, W.C., Fernandes, E.H., Monteiro, I.O., Moller, O.O., 2009. Numerical modeling of the Patos Lagoon coastal plume. Continent. Shelf Res. 29, 556–571. https://doi.org/10.1016/j.csr.2008.09.022.

Marques, W.C., Fernandes, E.H., Moraes, B.C., Moller, O.O., Malcherek, A., 2010. Dynamics of the Patos Lagoon coasta plume and its contribution to the deposition pattern of the South Brazilian inner shelf. J. Geophys. Res. 115, C10. https://doi.org/10.1029/2010JC006150.

Nash, J.D., Moum, J.N., 2005. River plumes as a source of large-amplitude internal waves in the coastal ocean. Nature 437, 400–403. https://doi.org/10.1038/nature03936.

Osadchiev, A., Izhitskiy, A., Zavialov, P., Kremenetskiy, V., Polukhin, A., Pelevin, V., Toktamysova, Zh, 2017. Structure of the buoyant plume formed by Ob and Yenisei river discharge in the southern part of the Kara Sea during summer and autumn. J. Geophys. Res. https://doi.org/10.1002/2016JC012603.

Palmer, S.C., Pelevin, V.V., Goncharenko, I.V., Kovács, A., Zlinszky, A., Présing, M., Horváth, H., Nicolás-Perea, V., Balzter, H., Tóth, V., 2013. Ultraviolet Fluorescence LiDAR (UFL) as a measurement tool for water quality parameters in turbid lake conditions. Rem. Sens. 5 (9), 4405–4422.

Pelevin, V., Zlinszky, A., Khimchenko, E., Toth, V., 2017. Ground truth data on chlorophyll-a, chromophoric dissolved organic matter and suspended sediment concentrations in the upper water layer as obtained by LIF LiDAR at high spatial resolution. Int. J. Rem. Sens. 38 (7), 1967–1982. https://doi.org/10.1080/01431161.2016.1274446.

Silva, P.D., Lisboa, P.V., Fernandes, E.H., 2015. Changes of the fine sediment dynamics after the Port of Rio Grande expansion. Adv. Geosci. 39, 123–127. https://doi.org/10.5194/adgeo-39-123-2015.

Zavialov, P.O., Kostianoy, A.G., Moller Jr., O.O., 2003. SAFARI cruise: mapping river discharge effects on Southern Brazilian shelf. Geophys. Res. Lett. 30, 21. https://doi.org/10.1029/2003GL018265.